

Contrasting electronic states of RuI₃ and RuCl₃

Lu Liu,^{1,2} Ke Yang,^{3,1} Guangyu Wang,^{1,2} Di Lu,^{1,2} Yaozhenghang Ma,^{1,2} and Hua Wu^{1,2,4,*}

¹Laboratory for Computational Physical Sciences (MOE), State Key Laboratory of Surface Physics, and Department of Physics, Fudan University, Shanghai 200433, China

²Shanghai Qi Zhi Institute, Shanghai 200232, China

³College of Science, University of Shanghai for Science and Technology, Shanghai 200093, China

⁴Collaborative Innovation Center of Advanced Microstructures, Nanjing 210093, China

(Dated: April 21, 2023)

The spin-orbital entangled states are of great interest as they hold exotic phases and intriguing properties. Here we use first-principles calculations to investigate the electronic and magnetic properties of RuI₃ and RuCl₃ in both bulk and monolayer cases. Our results show that RuI₃ bulk is a paramagnetic metal, which is in agreement with recent experiments. We find that the Ru³⁺ ion of RuI₃ is in the spin-orbital entangled $j_{\text{eff}} = \frac{1}{2}$ state. More interestingly, a metal-insulator transition occurs from RuI₃ bulk to monolayer, and this is mainly due to the band narrowing with the decreasing lattice dimensionality and to the Ru-I hybridization altered by the I 5*p* spin-orbit coupling. In contrast, RuCl₃ bulk and monolayer both show Mott-insulating behavior, the Ru³⁺ ion is in the formal $S = \frac{1}{2}$ and $L = 1$ state with a large in-plane orbital moment, and this result well explains the experimental large effective magnetic moment of RuCl₃ and the strong in-plane magnetization. The present work demonstrates the contrasting spin-orbital states and the varying properties of RuI₃ and RuCl₃.

I. INTRODUCTION

A wide variety of degrees of freedom, such as crystal field, electron correlation, and spin-orbit coupling (SOC), yield intriguing electronic structures and offer appealing opportunities for novel phenomena and rich properties. In particular, spin-orbital entangled states introduced by the SOC effect have been a hot topic and attracted a vast range of interests in the field of superconductivity, topological phases, quantum spin liquid, and exotic magnetism¹⁻⁵. Among them, the noted $j_{\text{eff}} = \frac{1}{2}$ state within the *d* *t*_{2*g*} subshell was first proposed to account for the Mott insulating behavior of Sr₂IrO₄⁶, and it is now widely used for the 4*d* and 5*d* transition metal compounds with significant SOC, to interpret their exotic electronic and magnetic properties. In addition, the spin-orbital entangled $j_{\text{eff}} = \frac{1}{2}$ pseudospin is suggested to accommodate bond dependent interaction in honeycomb lattice⁷⁻⁹, such as RuCl₃^{3,10}, Na₂IrO₃¹¹, and Na₃Co₂SbO₆¹², and it is extensively studied in the realization of the Kitaev model. Such novel spin-orbital states, driven by the delicate interplay of various degrees of freedom, provide room for exploring fundamental physics and potential applications.

As a potential candidate to realize a quantum spin liquid state under application of specific magnetic field strengths and directions, RuCl₃ is a quasi two dimensional (2D) material, in which the honeycomb layers are coupled by weak van der Waals (vdW) interaction, providing a high possibility to be cleaved into monolayer form with possibly exotic phases. Experimental results reveal that RuCl₃ bulk is a Mott insulator with planar zigzag antiferromagnetic (AFM) order of T_N ~ 7-14 K^{3,10,13-20}. As a close analog to RuCl₃, RuI₃ bulk has been synthesized very recently^{21,22}. Albeit the same honeycomb lattice and the Ru³⁺ 4*d*⁵ state, RuI₃ is a paramagnetic (PM) metal^{21,22}, showing contrasting elec-

tronic and magnetic properties from RuCl₃. Theoretical studies suggest that strong Ru 4*d*-I 5*p* hybridization and weak correlation effect account for the measured metallic behavior²³. It was also proposed that RuI₃ bulk is a bad metal and is on the verge of the metal-insulator transition²⁴. The contrasting electronic and magnetic behavior of bulk RuI₃ and RuCl₃ stimulate us to study their electronic states, particularly the spin-orbital states out of the intricate interplay of orbital hybridization, crystal field, electron correlation, and SOC.

In this work, using first-principles calculations, we investigate the electronic and magnetic properties of RuI₃ and RuCl₃ both in bulk and monolayer forms. Our results show that RuI₃ is in the PM state due to the strong Ru 4*d*-I 5*p* hybridization which suppresses the local Ru 4*d* Hund exchange. These results agree with the experimental and theoretical PM and bad-metallic behavior of RuI₃ bulk.²¹⁻²⁴ We find that the Ru³⁺ 4*d*⁵ ion is in the $j_{\text{eff}} = \frac{1}{2}$ state, and predict that RuI₃ undergoes a metal-insulator transition from bulk to monolayer. Moreover, we find that the Ru³⁺ ion in RuCl₃ bulk and monolayer is in the $S = \frac{1}{2}$ and $L = 1$ state with a large in-plane orbital moment. This result well accounts for experimental observations of the large effective magnetic moment and strong in-plane magnetization in RuCl₃.^{3,13,14,17} Thus, we have identified the contrasting electronic structures and magnetic properties for RuI₃ and RuCl₃.

II. COMPUTATIONAL DETAILS

Density functional theory calculations are carried out using the full-potential augmented plane wave plus local orbital code (WIEN2K)²⁵. Here we adopt the experimental $R\bar{3}21$ structure for RuI₃ bulk and the *C*2/*m*^{15,17,18} one for RuCl₃ bulk, both of which have the common edge-sharing octahedra (RuI₆ vs RuCl₆) forming a planar hon-

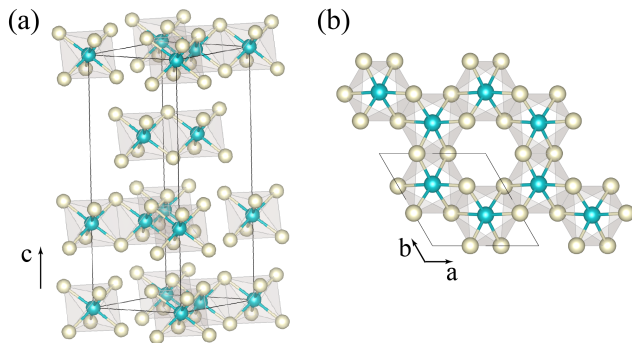


FIG. 1. The crystal structure of RuI_3 bulk (a) and monolayer (b): Ru (I) atoms are indicated by blue (yellow) balls.

eycomb lattice but have the different stacking orderings. As an example, we show the $R\bar{3}$ crystal structure of RuI_3 bulk in Fig. 1. The optimized lattice constants of RuI_3 bulk (monolayer) are $a=b=6.861$ (6.667) Å and $c=18.839$ Å, which are almost the same (within $\sim 1\%$) as the experimental ones of $a=b=6.791$ Å and $c=19.026$ Å²¹. And for RuCl_3 bulk (monolayer), the optimized parameters are $a=5.875$ (5.769) Å, $b=10.167$ (10.023) Å and $c=5.911$ Å, and they also agree well (within $\sim 1.7\%$) with the experimental ones of $a=5.976$ Å, $b=10.342$ Å and $c=6.013$ Å¹⁵. We also consider the $P3_1$ ¹² and $R\bar{3}$ ¹⁹ structures for RuCl_3 bulk, and find that they yield very similar results with the $C2/m$ one; see the Supplemental Material (SM)²⁶. The muffin-tin sphere radii are chosen to be 2.2, 2.4, and 2.1 bohrs for Ru, I, and Cl atoms, respectively. The cutoff energy of 14 Ry is used for plane wave expansion. The integration over the first Brillouin zone is performed using an $11 \times 11 \times 3$ ($9 \times 5 \times 9$) and $11 \times 11 \times 1$ ($9 \times 5 \times 1$) k-mesh for RuI_3 (RuCl_3) bulk and monolayer, respectively. The electron correlation effect is included by using the local spin density approximation plus Hubbard U (LSDA+ U) method²⁷. $U = 2$ eV and the Hund exchange $J_H = 0.5$ eV are used for the Ru 4d electrons^{23,24}. The SOC is included by the second variational method with scalar relativistic wave functions. We also perform calculations using the generalized gradient approximation (GGA)²⁸ for the exchange correlation functional, and find that the GGA gives quite similar results to the LDA for both RuI_3 and RuCl_3 in bulk and monolayer; see the SM²⁶.

III. RESULTS

A. RuI_3 bulk: $j_{\text{eff}} = \frac{1}{2}$ PM metallic state

We first investigate RuI_3 bulk to understand the $\text{Ru}^{3+} 4d^5$ state and the electronic and magnetic properties. To estimate the crystal field effect, we carry out spin-restricted LDA calculations. As shown in Fig. 2, the large t_{2g} - e_g splitting of about 2.0 eV makes the unoccupied e_g states lie above the Fermi level by about 1.8 eV, and the partially occupied t_{2g} states cross the Fermi

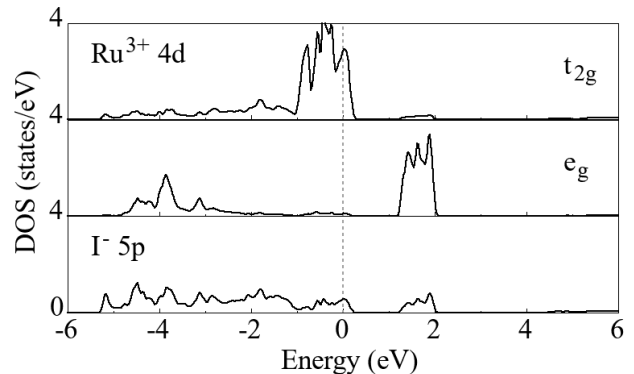


FIG. 2. The DOS result of RuI_3 bulk by LDA. The Fermi level is set at the zero energy.

level, showing the formal $\text{Ru}^{3+} t_{2g}^5$ configuration. Besides, the spatially extended I 5p orbitals have strong hybridization with Ru 4d ones, making the Ru 4d-I 5p states below the Fermi level distribute over the large energy range more than 5 eV. It is worth noting that the t_{2g}^5 state may carry an unquenched orbital angular momentum and the SOC strength is normally significant for Ru 4d electrons. Therefore, the SOC effect of the Ru 4d states (and of the I 5p orbitals) would be of concern.

We now carry out LDA+SOC calculations to see the SOC effect in RuI_3 . As shown in Fig. 3(a), in the presence of SOC, t_{2g} orbitals split into a lower $j_{\text{eff}} = \frac{3}{2}$ quartet and a higher $j_{\text{eff}} = \frac{1}{2}$ doublet. For the t_{2g}^5 configuration, four electrons fully occupy the $j_{\text{eff}} = \frac{3}{2}$ states, and the remaining one gives the half-filled $j_{\text{eff}} = \frac{1}{2}$ band across the Fermi level. While there are mixtures of $j_{\text{eff}} = \frac{1}{2}$ and $j_{\text{eff}} = \frac{3}{2}$, which are contributed by hybridization of Ru 4d and I 5p orbitals and local distortions away from perfect cubic conditions, those bands near the Fermi level are predominantly from the $j_{\text{eff}} = \frac{1}{2}$ states, and the bands in the range of 0.2-1.0 eV below Fermi level mostly consist of $j_{\text{eff}} = \frac{3}{2}$ states. Those separate bands via the splitting of $j_{\text{eff}} = \frac{1}{2}$ and $j_{\text{eff}} = \frac{3}{2}$ show the notable SOC effect of the $\text{Ru}^{3+} t_{2g}^5$ electrons.

Then we perform LSDA+SOC and LSDA+SOC+ U calculations to check the possible effect of Hund's exchange coupling and the moderate electron correlation. For RuI_3 bulk, we test a ferromagnetic state using LSDA+SOC, but it turns out to be unstable and converges to the same nonmagnetic state as the above LDA+SOC solution. In this sense, the Hund exchange is ineffective in RuI_3 bulk, which seems to be suppressed by the strong Ru 4d-I 5p band hybridizations. Then we probe the electron correlation effect using LSDA+SOC+ U calculations. We consider the nonmagnetic, ferromagnetic, and zigzag AFM configurations. All these states turn out to have a very close total energy within 0.4 meV/f.u., and the ferromagnetic and the zigzag AFM states have only a small magnetic moment of about $0.1 \mu_B/\text{Ru}$. Those results indicate that RuI_3 bulk is nonmagnetic rather than magnetic, and the elec-

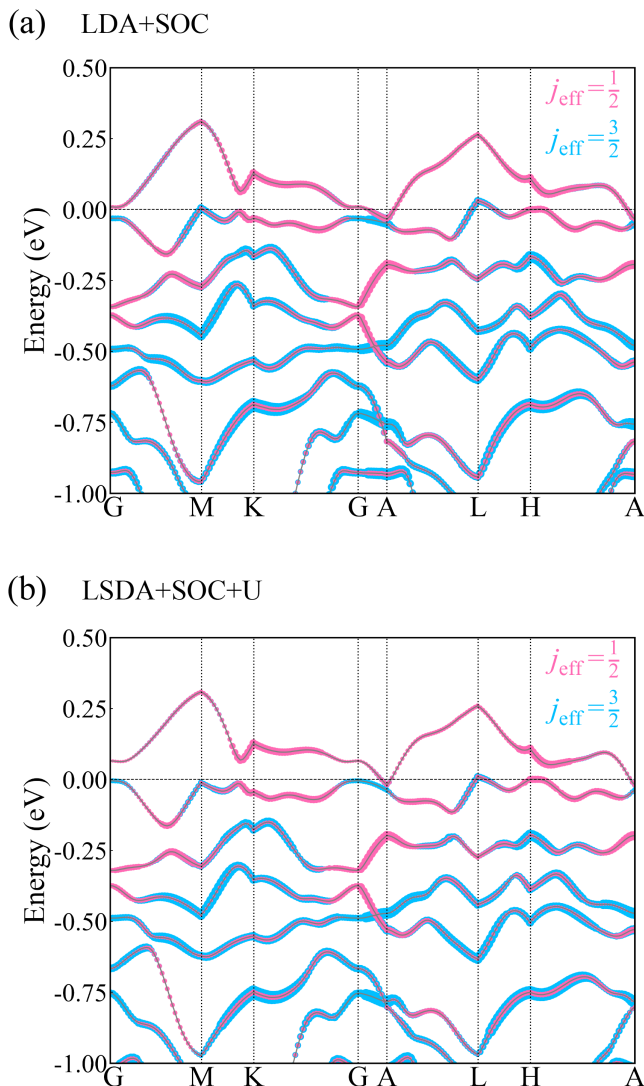


FIG. 3. The $j_{\text{eff}} = \frac{1}{2}$ (represented by pink curves) and $j_{\text{eff}} = \frac{3}{2}$ (blue curves) decomposed band structures of (a) LDA+SOC and (b) LSDA+SOC+U for RuI_3 bulk in the nonmagnetic state. The Fermi level is set at the zero energy.

tron correlation effect is insignificant by a comparison of the band structures shown in Figs. 3(a) and 3(b). The present nonmagnetic and metallic solution is largely ascribed to the strong Ru $4d$ -I $5p$ hybridizations and thus the delocalization behavior of the Ru $4d$ electrons. Therefore, our results well reproduce the experimental PM and bad-metallic behavior of RuI_3 bulk^{21,22} which is on the verge of the metal-insulator transition²⁴, and show that RuI_3 is in the spin-orbital entangled $j_{\text{eff}} = \frac{1}{2}$ state.

B. RuI_3 monolayer: $j_{\text{eff}} = \frac{1}{2}$ PM insulating state

As a quasi 2D material, RuI_3 bulk may be cleaved into the monolayer form. Using the DFT+vdW correction²⁹, the cleavage energy is calculated to be 0.24 J/m^2 , and it is even smaller than that³⁰ of 0.3 J/m^2 for CrI_3 which is

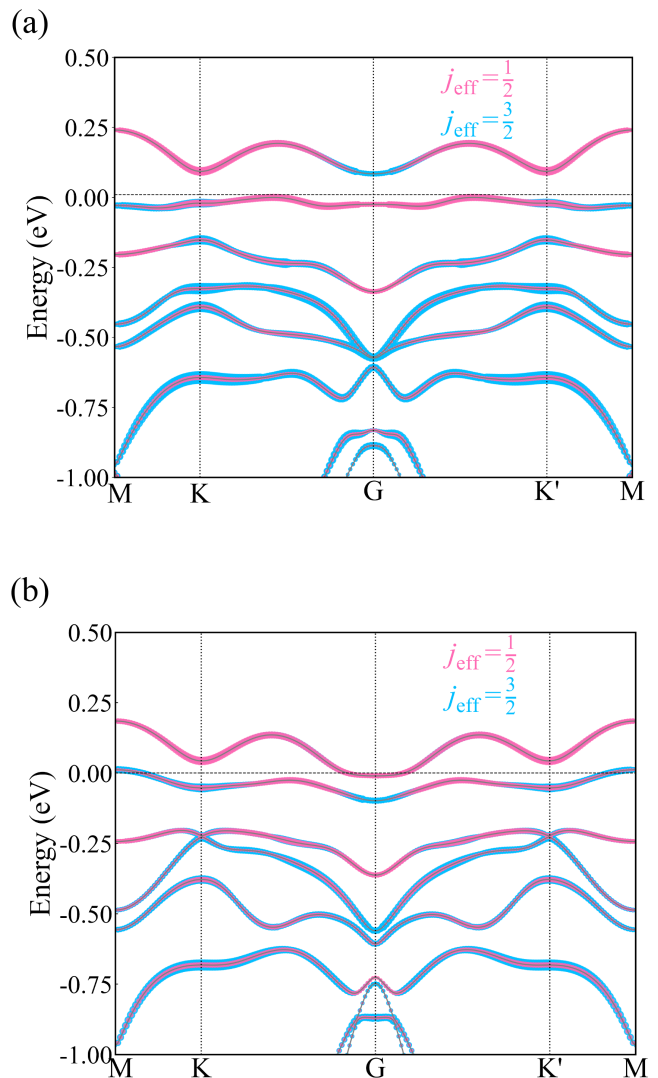


FIG. 4. The $j_{\text{eff}} = \frac{1}{2}$ (represented by pink curves) and $j_{\text{eff}} = \frac{3}{2}$ (blue curves) decomposed band structures of LDA+SOC for RuI_3 monolayer. (a) Both the Ru and I SOC are included. (b) The I SOC is inactive and only Ru SOC is active. The Fermi level is set at the zero energy.

already successfully cleaved by mechanical exfoliation³¹. Thus, we are now motivated to study the electronic and magnetic properties of the RuI_3 monolayer. Again, both the LDA+SOC and LSDA+SOC calculations give the same nonmagnetic solution. In contrast to the above nonmagnetic metallic state for RuI_3 bulk [Fig. 3(a)], the present nonmagnetic solution for the RuI_3 monolayer has now an insulating gap as seen in Fig. 4(a). In this sense, RuI_3 undergoes an interesting metal-insulator transition from bulk to monolayer. Besides the common reason of the band narrowing for gap opening due to the reduced dimensionality in the monolayer, the SOC effect of the I $5p$ orbital is found to be an important reason via the strong Ru $4d$ -I $5p$ hybridization. By a comparison between Figs. 4(a) and 4(b), we find that when the I $5p$ SOC is switched off in the LDA+SOC calculations, the

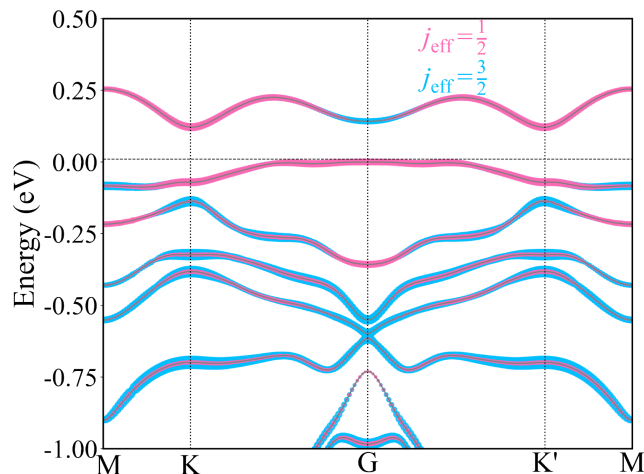


FIG. 5. The $j_{\text{eff}} = \frac{1}{2}$ (represented by pink curves) and $j_{\text{eff}} = \frac{3}{2}$ (blue curves) decomposed band structure of LSDA+SOC+ U for RuI₃ monolayer. The Fermi level is set at the zero energy.

two bands of the $j_{\text{eff}} = \frac{1}{2}$ subset around the Fermi level change a lot in energy dispersion and band shift, and they restore the metallic behavior. Note that for a typical $j_{\text{eff}} = \frac{1}{2}$ magnetic Mott insulator like Sr₂IrO₄, the half-filled $j_{\text{eff}} = \frac{1}{2}$ band undergoes a split and opens an insulating gap by a Hubbard U . In strong contrast, here for the nonmagnetic insulating RuI₃ monolayer, the gap opening is not due to a Hubbard U , but to the band narrowing in the reduced dimensionality and to the band tuning of the strong Ru $4d$ -I $5p$ hybridization by the I $5p$ SOC effect.

Now we check the possible effects of the Hubbard U on the electronic and magnetic structures of the RuI₃ monolayer. By carrying out LSDA+SOC+ U calculations, we can stabilize the nonmagnetic, ferromagnetic, and zigzag AFM solutions, respectively. Our results show that all these three solutions are in the $j_{\text{eff}} = \frac{1}{2}$ state, and that the ferromagnetic (zigzag AFM) state has the local spin/orbital moment of 0.50/0.22 (0.42/0.44) μ_{B} /Ru. It is important to note that the nonmagnetic state is most stable and it has a lower total energy than the zigzag AFM and ferromagnetic states by 2.7 and 15.1 meV/f.u., respectively. The nonmagnetic insulating gap is slightly increased by the Hubbard U ; see Figs. 4(a) and (5). This nonmagnetic $j_{\text{eff}} = \frac{1}{2}$ insulating state is much different from the typical magnetic $j_{\text{eff}} = \frac{1}{2}$ Mott-insulating state, e.g., in Sr₂IrO₄⁶. The latter has a formal local spin (orbital) moment of 0.33 (0.67) μ_{B} , and its Mott gap is opened by the correlation effect in the half-filled $j_{\text{eff}} = \frac{1}{2}$ doublet. For the RuI₃ monolayer, it is found to be a nonmagnetic $j_{\text{eff}} = \frac{1}{2}$ insulator, and its gap opening is mainly due to the band effect of the strong Ru $4d$ -I $5p$ hybridization with the significant SOC, rather than the electron correlation effect, as proven in the above calculations. In this respect, the previous theoretical suggestion of a ferromagnetic behavior^{32,33} for the insulating RuI₃ monolayer seems at odd with the experimental PM behavior of RuI₃ bulk,^{21,22} as the weak interlayer vdW in-

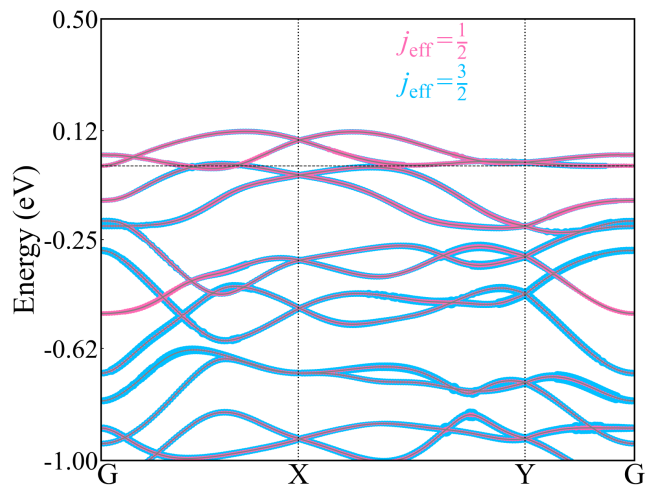


FIG. 6. The $j_{\text{eff}} = \frac{1}{2}$ (represented by pink curves) and $j_{\text{eff}} = \frac{3}{2}$ (blue curves) decomposed band structure of LDA+SOC for RuCl₃ bulk. The Fermi level is set at the zero energy.

teraction normally would not change the intralayer magnetism drastically. Therefore, our present result of the nonmagnetic behavior for the RuI₃ monolayer would be more reasonable.

So far, using the first principles calculations, we have well explained the experimental PM metallic state of RuI₃ bulk^{21,22}, and have predicted the interesting nonmagnetic insulating state for the RuI₃ monolayer. Both the bulk and monolayer RuI₃ are in the $j_{\text{eff}} = \frac{1}{2}$ state due to the strong Ru $4d$ SOC. But an interesting metal-insulator transition occurs from the bulk to monolayer, and it is mainly due to the band narrowing in the reduced dimensionality and to the band tuning of the strong Ru $4d$ -I $5p$ hybridization by the I $5p$ SOC effect.

C. RuCl₃ bulk: $S = \frac{1}{2}$ and $L = 1$ Mott-insulating state

Comparing with RuI₃, RuCl₃ has a similar honeycomb lattice and the same Ru³⁺ $4d^5$ configuration, but has totally contrasting electronic and magnetic properties, being a Mott insulator with zigzag AFM order and strong in-plane magnetic anisotropy^{3,10,13-19}. This implies diverse spin-orbital states through interplay of various degrees of freedom. Hence, we are motivated to investigate the electronic structures of RuCl₃ bulk. First, in the LDA+SOC framework, the Ru³⁺ ion of RuCl₃ bulk is in the $j_{\text{eff}} = \frac{1}{2}$ state due to the significant SOC effect of Ru $4d$ electrons, and the $j_{\text{eff}} = \frac{1}{2}$ bands cross the Fermi level; see Fig. 6. The $j_{\text{eff}} = \frac{1}{2}$ metallic behavior is similar to the situation in RuI₃ bulk [Fig. 3(a)].

However, when including Hund's coupling, the electronic state undergoes a drastic change: the Ru $4d$ electrons in RuCl₃ prefer to be spin polarized, in stark contrast with the PM character of RuI₃. Now the zigzag AFM state of RuCl₃ bulk with the easy in-plane magne-

tization (see below) is calculated by LSDA+SOC to be more stable than the nonmagnetic one by 15.6 meV/f.u., and has a local spin moment of $0.59 \mu_B/\text{Ru}$. This suggests that the Hund exchange is effective in RuCl_3 , which should arise from the stronger ionic behavior and the weaker covalence effect in RuCl_3 than in RuI_3 .

To show the collective effects of crystal field, SOC, Hund's coupling, and electronic correlation, we then perform LSDA+SOC+ U calculations. Indeed, the zigzag AFM state is more stable than the nonmagnetic one by 117.7 meV/f.u., showing the strong effects of Hund's exchange and electron correlation. In addition to the local spin moment of $0.70 \mu_B/\text{Ru}$, the Ru^{3+} ion in RuCl_3 bulk also has an in-plane orbital moment of $0.47 \mu_B/\text{Ru}$. This state with such a large spin and orbital moment then questions the $j_{\text{eff}} = \frac{1}{2}$ description in RuCl_3 , as the $j_{\text{eff}} = \frac{1}{2}$ state has a spin moment of $0.33 \mu_B$ and orbital moment of $0.67 \mu_B$. In fact, the nature of the $j_{\text{eff}} = \frac{1}{2}$ basis in RuCl_3 remains controversial. In experiments, strong magnetic anisotropy is observed and the g factors are estimated to be $g_{ab} \sim 2.5$ and $g_c \sim 0.4$ ¹⁶, whereas theoretical studies demonstrate that the pure $j_{\text{eff}} = \frac{1}{2}$ state (i.e., no mixture with $j_{\text{eff}} = \frac{3}{2}$) has isotropic orbital nature and gives isotropic g factors. Besides, the experimental magnetic moment of $\sim 1.2 \mu_B/\text{Ru}$ under an in-plane magnetic field of 60 T is not yet saturated^{15,16} but is already larger than the total magnetic moment of $1 \mu_B$ either in the $j_{\text{eff}} = \frac{1}{2}$ state or in the pure $S = \frac{1}{2}$ state. This indicates a large contribution from the orbital moment, and the in-plane moment of $\sim 1.2 \mu_B/\text{Ru}$ can be explained by the above calculated spin moment of $0.70 \mu_B$ plus the orbital moment of $0.47 \mu_B$. Moreover, the experimental effective magnetic moment (μ_{eff}) of 2.0-2.4 μ_B for in-plane magnetization^{3,13,14,17} is also much larger than that of 1.73 μ_B for the $j_{\text{eff}} = \frac{1}{2}$ state. Furthermore, theoretical studies suggest that local distortions and energy splitting, e.g., splitting via trigonal crystal field, would alter orbital and spin components of $j_{\text{eff}} = \frac{1}{2}$ basis and bring about anisotropic behavior^{16,34,35}. Those experimental and theoretical works indicate that the $j_{\text{eff}} = \frac{1}{2}$ picture of RuCl_3 may need a reconsideration. As seen below, indeed we find that owing to the considerable Hund's coupling, moderate SOC, and trigonal crystal field splitting, RuCl_3 bulk is in the $S = \frac{1}{2}$ and $L_x = 1$ state with in-plane anisotropy rather than the $j_{\text{eff}} = \frac{1}{2}$ state.

Considering the trigonal crystal field, the t_{2g} triplet would split into the a_{1g} singlet and e'_g doublet^{36,37}. Using the global coordinate system with z axis along the octahedral [111] direction and y along the [1 $\bar{1}$ 0] direction, the wave functions of t_{2g} orbitals can be written as

$$\begin{aligned} |a_{1g}\rangle &= |3z^2 - r^2\rangle \\ |e'_{g1}\rangle &= \sqrt{\frac{2}{3}}|x^2 - y^2\rangle - \sqrt{\frac{1}{3}}|xz\rangle \\ |e'_{g2}\rangle &= \sqrt{\frac{2}{3}}|xy\rangle + \sqrt{\frac{1}{3}}|yz\rangle. \end{aligned} \quad (1)$$

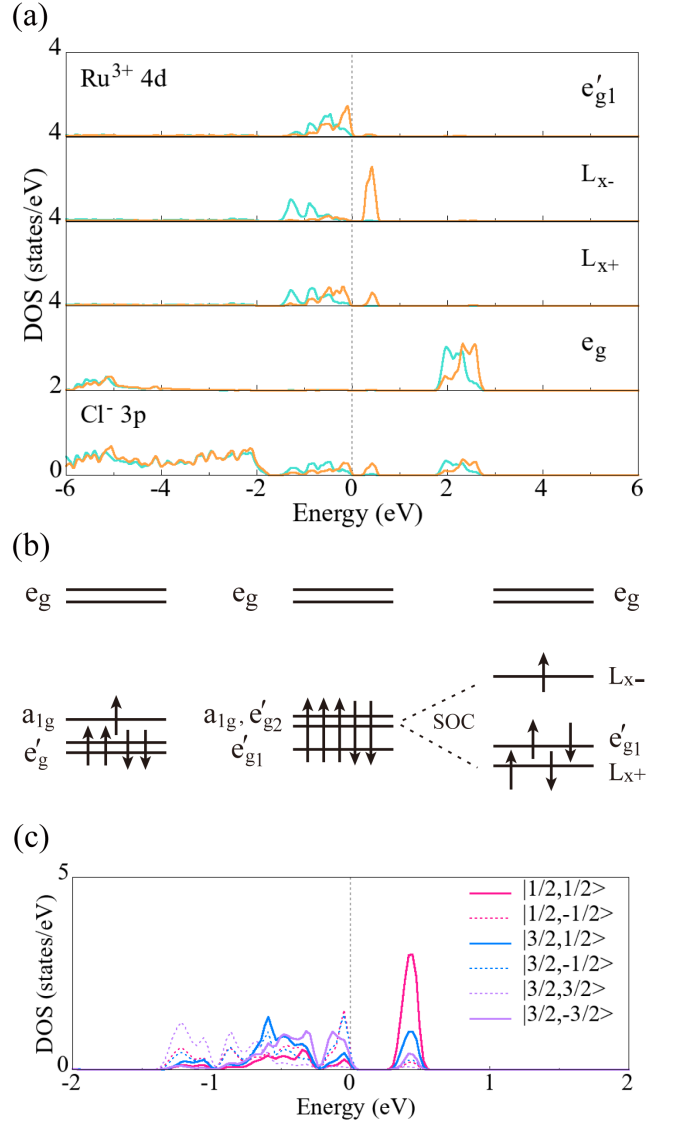


FIG. 7. (a) The DOS result of LSDA+SOC+ U for RuCl_3 bulk. The Ru^{3+} ions in zigzag antiferromagnetic order with spins along x axis have each the $t_{2g}^3 e'_{g1} L_{x+}$ configuration. The green (orange) curves refer to up (down) spins. The Fermi level is set at the zero energy. (b) The trigonal crystal field level diagrams, and the SOC mixing of a_{1g} and e'_{g2} to yield the $L_{x\pm}$ states. (c) The t_{2g} states in (a) are projected onto the $|j_{\text{eff}}, m_j^x\rangle$ basis.

For the spins aligning in the ab plane, for example, along the x axis, SOC would mix a_{1g} and e'_{g2} orbitals to produce the $L_{x\pm}$ ($L_x = \pm 1$) states^{38,39}

$$|L_x = \pm 1\rangle = \sqrt{\frac{1}{2}}(i|e'_{g2}\rangle \mp |a_{1g}\rangle). \quad (2)$$

Using this basis, the decomposed DOS results are shown in Fig. 7(a). The Ru^{3+} ion in RuCl_3 has a moderate exchange splitting of about 0.2 eV, which is somewhat larger than the SOC strength $\lambda \sim 0.1$ eV for Ru 4d electrons^{17,34,40,41}. With the assistance of Hund's cou-

pling, the $t_{2g}^{3\uparrow 2\downarrow}$ configuration is produced. Then the two spin-down electrons occupy the e'_{g1} and L_{x+} states to gain the SOC splitting energy and produce the $S = \frac{1}{2}$ and $L_x = 1$ state; see Fig. 7(a) and (b). A Mott gap is opened by the correlation effect.

We also check the $j_{\text{eff}} = \frac{1}{2}$ basis by projecting the above $S = \frac{1}{2}$ and $L_x = 1$ state (Fig. 7(a)) onto the $|j_{\text{eff}}, m_j^x\rangle$ orbitals which have the forms as follows:

$$\begin{aligned}
\left|\frac{1}{2}, \frac{1}{2}\right\rangle &= -\sqrt{\frac{2}{3}}|L_x = -1, \downarrow\rangle + \sqrt{\frac{1}{3}}|e'_{g1}, \uparrow\rangle \\
\left|\frac{1}{2}, -\frac{1}{2}\right\rangle &= -\sqrt{\frac{2}{3}}|L_x = +1, \uparrow\rangle + \sqrt{\frac{1}{3}}|e'_{g1}, \downarrow\rangle \\
\left|\frac{3}{2}, \frac{3}{2}\right\rangle &= |L_x = -1, \uparrow\rangle \\
\left|\frac{3}{2}, -\frac{3}{2}\right\rangle &= |L_x = +1, \downarrow\rangle \\
\left|\frac{3}{2}, \frac{1}{2}\right\rangle &= \sqrt{\frac{1}{3}}|L_x = -1, \downarrow\rangle + \sqrt{\frac{2}{3}}|e'_{g1}, \uparrow\rangle \\
\left|\frac{3}{2}, -\frac{1}{2}\right\rangle &= \sqrt{\frac{1}{3}}|L_x = +1, \uparrow\rangle + \sqrt{\frac{2}{3}}|e'_{g1}, \downarrow\rangle.
\end{aligned} \tag{3}$$

The DOS results are shown in Fig. 7(c). We find that the $j_{\text{eff}} = \frac{1}{2}$ and $j_{\text{eff}} = \frac{3}{2}$ states have significant mixtures, and this was also found in previous works^{15,42}. The mixture may also be partially due to the Ru-Ru intersite hopping and the band formation⁴³⁻⁴⁵. Moreover, we test the increasing U values of 3 eV and 4 eV to see a possible influence of the enhanced atomic effect (and reducing band hybridization) on the $j_{\text{eff}} = \frac{1}{2}$ picture, but we find that the $S = \frac{1}{2}$ and $L_x = 1$ state persists and thus the strong mixture between the $j_{\text{eff}} = \frac{1}{2}$ and $j_{\text{eff}} = \frac{3}{2}$ remains, as seen in Fig. S4 in the SM²⁶. Note that the t_{2g} hole state $|L_x = -1, \downarrow\rangle$ in Fig. 7(a) can be written as

$$|L_x = -1, \downarrow\rangle = -\sqrt{\frac{2}{3}}\left|\frac{1}{2}, \frac{1}{2}\right\rangle + \sqrt{\frac{1}{3}}\left|\frac{3}{2}, \frac{1}{2}\right\rangle. \tag{4}$$

Indeed, this composition of the t_{2g} hole state is clearly seen in Fig. 7(c), and thus the $j_{\text{eff}} = \frac{1}{2}$ state seems not to be a good eigenstate. We still attempt to obtain the $j_{\text{eff}} = \frac{1}{2}$ eigenstate in our LSDA+SOC+ U calculations by setting the corresponding occupation density matrix, however, it eventually converges to the $S = \frac{1}{2}$ and $L_x = 1$ state. All these results suggest that with a considerable Hund exchange, trigonal crystal field splitting, and moderate SOC, the $j_{\text{eff}} = \frac{1}{2}$ state could not be the most suitable picture for RuCl₃.

Moreover, we test other configurations for the Ru³⁺ t_{2g}^5 electrons. For example, when we set the spins along the z axis, we will get the $S = \frac{1}{2}$ and $L_z = 1$ state via the SOC-mixing of e'_{g1} and e'_{g2} orbitals. However, this state has a higher total energy than the $S = \frac{1}{2}$ and $L_x = 1$ state by 26.7 meV/f.u. This accords with the experimental easy in-plane magnetization and the larger

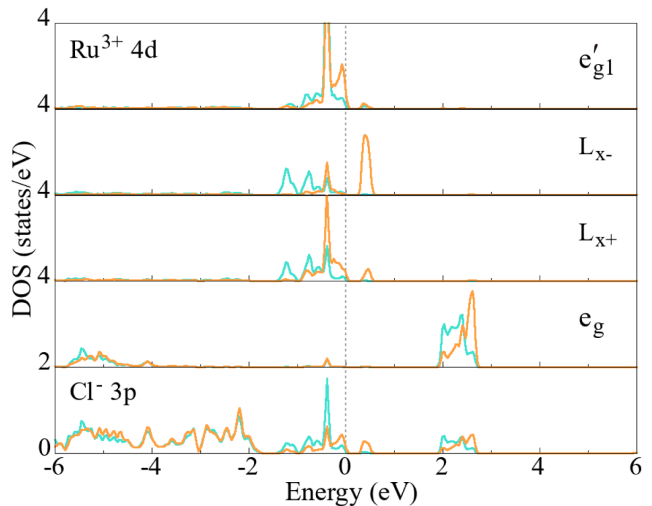


FIG. 8. The DOS result of LSDA+SOC+ U for RuCl₃ monolayer. The green (orange) curves refer to up (down) spins. The Fermi level is set at the zero energy.

in-plane g factor than the out-of-plane one¹³⁻¹⁶. Therefore, our results show that RuCl₃ bulk is a Mott insulator in the formal $S = \frac{1}{2}$ and $L = 1$ state with the easy in-plane magnetization, and the in-plane effective moment $\mu_{\text{eff}} = \sqrt{g_s^2 S(S+1) + g_l^2 L(L+1)} \approx 2.24 \mu_B$ could well account for the experimental one of 2.0-2.4 μ_B ^{3,13,14,17}. Our results provide new perspectives to understand the electronic and magnetic properties of RuCl₃.

D. RuCl₃ monolayer: $S = \frac{1}{2}$ and $L = 1$ Mott-insulating state

The cleavage energy for RuCl₃ monolayers is calculated by the DFT+vdW correction to be 0.17 J/m², and it is even smaller than that of 0.24 for RuI₃ monolayers and 0.3 J/m² for CrI₃ monolayers. We now explore the electronic and magnetic properties of the RuCl₃ monolayer. The calculated electronic structures are very similar to RuCl₃ bulk and are thus not described here in a repeated way. We just stress the LSDA+SOC+ U results (see Fig. 8), which confirm that the RuCl₃ monolayer is a Mott insulator in the formal $S = \frac{1}{2}$ and $L = 1$ state with the easy in-plane magnetization. The zigzag AFM state is more stable than the nonmagnetic one by 130.8 meV/f.u., and it has a local spin moment of 0.70 μ_B /Ru and an in-plane orbital moment of 0.46 μ_B /Ru.

IV. SUMMARY

In light of all the above results, we find that RuI₃ and RuCl₃ display contrasting electronic and magnetic properties due to a delicate interplay of SOC, Hund's coupling, crystal field effect, transition metal-ligand hybridization, and electron correlation. When one considers the SOC effect of Ru $4d$ electrons in the local octahedral

crystal field, the splitting of $j_{\text{eff}} = \frac{1}{2}$ and $j_{\text{eff}} = \frac{3}{2}$ orbitals would give the half-filled $j_{\text{eff}} = \frac{1}{2}$ bands for the $\text{Ru}^{3+} t_{2g}^5$ configuration. This scenario is the same for both RuI_3 and RuCl_3 . However, when including the effect of Hund's coupling, we find that RuI_3 tends to be in the nonmagnetic state whereas RuCl_3 prefers to be in the spin-polarized zigzag AFM state. It is not surprising, given that for RuI_3 , the lower electronegativity of the ligand iodine and its wide $5p$ orbital give rise to stronger Ru $4d$ -I $5p$ hybridization, and thus to the stronger delocalization behavior and weaker spin polarization for Ru^{3+} $4d$ electrons compared with those in RuCl_3 . As a result, with the assistance of dominant SOC and negligible Hund's coupling, the RuI_3 bulk and monolayer are in the spin-orbital entangled $j_{\text{eff}} = \frac{1}{2}$ nonmagnetic state. Moreover, aided by the strong SOC of I $5p$ orbitals and their hybridization with Ru $4d$ orbitals, the RuI_3 monolayer displays the $j_{\text{eff}} = \frac{1}{2}$ band insulating behavior. In contrast, the RuCl_3 bulk and monolayer have considerable Hund's exchange splitting which is somewhat larger than the SOC strength, and combined with moderate trigonal crystal field splitting, they tend to have a large spin and in-plane orbital moment, thus approaching the formal $S = \frac{1}{2}$ and $L = 1$ state rather than the $j_{\text{eff}} = \frac{1}{2}$ state. Moreover, the electron correlation opens a Mott-insulating gap for more ionic RuCl_3 with stronger electron localization. Then, these results for RuCl_3 well account for the experimental effective magnetic moment, the large in-plane magnetic moment and in-plane anisotropy¹³⁻¹⁷. Therefore, albeit the same t_{2g}^5 configuration, the contrasting electronic structures in RuI_3 and RuCl_3 give rise to the varying electronic and magnetic properties: RuI_3 bulk is a PM bad metal and RuCl_3 bulk is a zigzag AFM Mott insulator. Our results well agree with those experiments^{3,10,13-19,21,22}. More-

over, we predict a metal-insulator transition for RuI_3 from bulk to monolayer, but the RuCl_3 monolayer persists in the Mott-insulating state.

In summary, using density functional calculations, we confirm that RuI_3 bulk is a PM bad metal^{21,22} on the verge of the metal-insulator transition²⁴ and has the Ru^{3+} spin-orbital entangled $j_{\text{eff}} = \frac{1}{2}$ state. Our results are consistent with the experimental observations. Moreover, a metal-insulator transition occurs for RuI_3 from bulk to monolayer, and the gap opening in the RuI_3 monolayer is mainly due to the band narrowing with the decreasing lattice dimensionality and to the altered Ru $4d$ -I $5p$ hybridization by the strong I $5p$ SOC effect. In contrast with the $j_{\text{eff}} = \frac{1}{2}$ state in RuI_3 , RuCl_3 turns out to be in the $S = \frac{1}{2}$ and $L = 1$ state with a stronger in-plane magnetic anisotropy. Its Mott-insulating state and the zigzag AFM state arise from the delicate interplay of electron correlation, Hund's coupling, SOC, and trigonal crystal field distortion. These results well explain the experimental effective magnetic moment and strong in-plane magnetization of RuCl_3 bulk. We conclude that the varying electronic and magnetic properties of RuI_3 and RuCl_3 are ascribed to the contrasting electronic structures, particularly the $j_{\text{eff}} = \frac{1}{2}$ state for the former, and the $S = \frac{1}{2}$ and $L = 1$ state for the latter. Thus this work highlights the distinct Ru^{3+} spin-orbital states and the importance of subtle interactions among various degrees of freedom.

ACKNOWLEDGEMENTS

This work was supported by the National Natural Science Foundation of China (Grants No. 12174062, No. 12241402, and No. 12104307).

* Corresponding author. wuh@fudan.edu.cn

¹ W. Witczak-Krempa, G. Chen, Y. B. Kim, and L. Balents, *Annu. Rev. Condens. Matter Phys.* **5**, 57 (2014).

² J. W. Harter, Z. Y. Zhao, J.-Q. Yan, D. G. Mandrus, and D. Hsieh, *Science* **356**, 295 (2017).

³ A. Banerjee, J. Yan, J. Knolle, C. A. Bridges, M. B. Stone, M. D. Lumsden, D. G. Mandrus, D. A. Tennant, R. Moessner, and S. E. Nagler, *Science* **356**, 1055 (2017).

⁴ Y. Kasahara, T. Ohnishi, Y. Mizukami, O. Tanaka, S. Ma, K. Sugii, N. Kurita, H. Tanaka, J. Nasu, Y. Motome, T. Shibauchi, and Y. Matsuda, *Nature* **559**, 227 (2018).

⁵ T. Yokoi, S. Ma, Y. Kasahara, S. Kasahara, T. Shibauchi, N. Kurita, H. Tanaka, J. Nasu, Y. Motome, C. Hickey, S. Trebst, and Y. Matsuda, *Science* **373**, 568 (2021).

⁶ B. J. Kim, H. Jin, S. J. Moon, J.-Y. Kim, B.-G. Park, C. S. Leem, J. Yu, T. W. Noh, C. Kim, S.-J. Oh, J.-H. Park, V. Durairaj, G. Cao, and E. Rotenberg, *Phys. Rev. Lett.* **101**, 076402 (2008).

⁷ G. Khaliullin, *Prog. Theor. Phys.* **160**, 155 (2005).

⁸ G. Jackeli and G. Khaliullin, *Phys. Rev. Lett.* **102**, 017205 (2009).

⁹ H. Takagi, T. Takayama, G. Jackeli, G. Khaliullin, and S. E. Nagler, *Nat. Rev. Phys.* **1**, 264 (2019).

¹⁰ S.-H. Do, S.-Y. Park, J. Yoshitake, J. Nasu, Y. Motome, Y. Kwon, D. T. Adroja, D. J. Voneshen, K. Kim, T.-H. Jang, J.-H. Park, K.-Y. Choi, and S. Ji, *Nature Phys.* **13**, 1079 (2017).

¹¹ S. Hwan Chun, J.-W. Kim, J. Kim, H. Zheng, C. Stoumpos, C. Malliakas, J. Mitchell, K. Mehlawat, Y. Singh, Y. Choi, T. Gog, A. Al-Zein, M. Sala, M. Krisch, J. Chaloupka, G. Jackeli, G. Khaliullin, and B. J. Kim, *Nature Phys.* **11**, 462 (2015).

¹² H. Liu, J. Chaloupka, and G. Khaliullin, *Phys. Rev. Lett.* **125**, 047201 (2020).

¹³ M. Majumder, M. Schmidt, H. Rosner, A. A. Tsirlin, H. Yasuoka, and M. Baenitz, *Phys. Rev. B* **91**, 180401(R) (2015).

¹⁴ J. A. Sears, M. Songvilay, K. W. Plumb, J. P. Clancy, Y. Qiu, Y. Zhao, D. Parshall, and Y.-J. Kim, *Phys. Rev. B* **91**, 144420 (2015).

¹⁵ R. D. Johnson, S. C. Williams, A. A. Haghighirad, J. Singleton, V. Zapf, P. Manuel, I. I. Mazin, Y. Li, H. O. Jeschke, R. Valentí, and R. Coldea, *Phys. Rev. B* **92**,

- 235119 (2015).
- 16 Y. Kubota, H. Tanaka, T. Ono, Y. Narumi, and K. Kindo, *Phys. Rev. B* **91**, 094422 (2015).
 - 17 A. Banerjee, C. A. Bridges, J.-Q. Yan, A. A. Aczel, L. Li, M. B. Stone, G. E. Granroth, M. D. Lumsden, Y. Yiu, J. Knolle, S. Bhattacharjee, D. L. Kovrizhin, R. Moessner, D. A. Tennant, D. G. Mandrus, and S. E. Nagler, *Nature Mater.* **15**, 733 (2016).
 - 18 H. B. Cao, A. Banerjee, J.-Q. Yan, C. A. Bridges, M. D. Lumsden, D. G. Mandrus, D. A. Tennant, B. C. Chakoumakos, and S. E. Nagler, *Phys. Rev. B* **93**, 134423 (2016).
 - 19 S. Y. Park, S. H. Do, K. Y. Choi, D. Jang, T. H. Jang, J. Schefer, C. M. Wu, J. S. Gardner, J. M. S. Park, J. H. Park, and S. Ji, [arXiv:1609.05690](https://arxiv.org/abs/1609.05690).
 - 20 S. Sinn, C. H. Kim, B. H. Kim, K. D. Lee, C. J. Won, J. S. Oh, M. Han, Y. J. Chang, N. Hur, H. Sato, B.-G. Park, C. Kim, H.-D. Kim, and T. W. Noh, *Sci. Rep.* **6**, 39544 (2016).
 - 21 D. Ni, X. Gui, K. M. Powderly, and R. J. Cava, *Adv. Mater.* **34**, 2106831 (2022).
 - 22 K. Nawa, Y. Imai, Y. Yamaji, H. Fujihara, W. Yamada, R. Takahashi, T. Hiraoka, M. Hagihala, S. Torii, T. Aoyama, T. Ohashi, Y. Shimizu, H. Gotou, M. Itoh, K. Ohgushi, and T. J. Sato, *J. Phys. Soc. Jpn.* **90**, 123703 (2021).
 - 23 Y. Zhang, L.-F. Lin, A. Moreo, and E. Dagotto, *Phys. Rev. B* **105**, 085107 (2022).
 - 24 D. A. S. Kaib, K. Riedl, A. Razpopov, Y. Li, S. Backes, I. Mazin, and R. Valentí, *npj Quantum Mater.* **7**, 75 (2022).
 - 25 P. Blaha, K. Schwarz, F. Tran, R. Laskowski, G. K. H. Madsen, and L. D. Marks, *J. Chem. Phys.* **152**, 074101 (2020).
 - 26 See Supplemental Material for (i) RuCl_3 bulk in $P3_112$ and $R\bar{3}$ structures, (ii) LSDA+SOC+U and GGA+SOC+U for RuI_3 , (iii) LSDA+SOC+U and GGA+SOC+U for RuCl_3 , and (iv) larger U values for RuCl_3 bulk.
 - 27 V. I. Anisimov, I. V. Solovyev, M. A. Korotin, M. T. Czyżyk, and G. A. Sawatzky, *Phys. Rev. B* **48**, 16929 (1993).
 - 28 J. P. Perdew, K. Burke, and M. Ernzerhof, *Phys. Rev. Lett.* **77**, 3865 (1996).
 - 29 K. Lee, E. D. Murray, L. Kong, B. I. Lundqvist, and D. C. Langreth, *Phys. Rev. B* **82**, 081101(R) (2010).
 - 30 M. A. McGuire, H. Dixit, V. R. Cooper, and B. C. Sales, *Chem. Mater.* **27**, 612 (2015).
 - 31 B. Huang, G. Clark, E. Navarro-Moratalla, D. R. Klein, R. Cheng, K. L. Seyler, D. Zhong, E. Schmidgall, M. A. McGuire, D. H. Cobden, W. Yao, D. Xiao, P. Jarillo-Herrero, and X. Xu, *Nature* **546**, 270 (2017).
 - 32 C. Huang, J. Zhou, H. Wu, K. Deng, P. Jena, and E. Kan, *Phys. Rev. B* **95**, 045113 (2017).
 - 33 F. Ersan, E. Vatanserver, S. Sarikurt, Y. Yüksel, Y. Kadioglu, H. D. Ozaydin, O. Üzengi Aktürk, Ümit Akıncı, and E. Aktürk, *J. Magn. Magn. Mater.* **476**, 111 (2019).
 - 34 S. M. Winter, A. A. Tsirlin, M. Daghofer, J. van den Brink, Y. Singh, P. Gegenwart, and R. Valentí, *J. Phys.: Condens. Matter* **29**, 493002 (2017).
 - 35 J. Chaloupka and G. Khaliullin, *Phys. Rev. B* **94**, 064435 (2016).
 - 36 D. I. Khomskii, *Transition Metal Compounds* (Cambridge University Press, 2014).
 - 37 K. Yang, F. Fan, H. Wang, D. I. Khomskii, and H. Wu, *Phys. Rev. B* **101**, 100402(R) (2020).
 - 38 L. Liu, K. Yang, G. Wang, and H. Wu, *J. Mater. Chem. C* **8**, 14782 (2020).
 - 39 D. Lu, L. Liu, Y. Ma, K. Yang, and H. Wu, *J. Mater. Chem. C* **10**, 8009 (2022).
 - 40 H.-S. Kim, V. Vijay Shankar, A. Catuneanu, and H.-Y. Kee, *Phys. Rev. B* **91**, 241110(R) (2015).
 - 41 A. Koitzsch, C. Habenicht, E. Müller, M. Knupfer, B. Büchner, H. C. Kandpal, J. van den Brink, D. Nowak, A. Isaeva, and T. Doert, *Phys. Rev. Lett.* **117**, 126403 (2016).
 - 42 R. Yadav, N. A. Bogdanov, V. M. Katukuri, S. Nishimoto, J. van den Brink, and L. Hozoi, *Sci. Rep.* **6**, 37925 (2016).
 - 43 H.-S. Kim, E. K.-H. Lee, and Y. B. Kim, *EPL* **112**, 67004 (2016).
 - 44 I. I. Mazin, H. O. Jeschke, K. Foyevtsova, R. Valentí, and D. I. Khomskii, *Phys. Rev. Lett.* **109**, 197201 (2012).
 - 45 X. Ou, Z. Li, F. Fan, H. Wang, and H. Wu, *Sci. Rep.* **4**, 7542 (2014).

Supplemental Material

I. RuCl₃ bulk in $P3_112$ and $R\bar{3}$ structures

In addition to the $C2/m$ structure calculated in the main text, here we also consider the $P3_112$ and $R\bar{3}$ structures for RuCl₃ bulk. The lattice constants are optimized to be $a=b=5.957$ Å and $c=17.183$ Å for the $P3_112$ structure, and $a=b=5.931$ Å and $c=17.095$ Å for the $R\bar{3}$ one. We find that the $P3_112$ and $R\bar{3}$ structures give very similar results with the $C2/m$ one. The LSDA+SOC+U calculations show that the Ru³⁺ ion has local spin moment of 0.70 (0.69) μ_B /Ru and an in-plane orbital moment of 0.54 (0.55) μ_B /Ru in $P3_112$ ($R\bar{3}$) structure, giving the $S = \frac{1}{2}$ and $L_x = 1$ state (see Fig. S1). The zigzag AF state is more stable than the nonmagnetic one by 124.9 (131.2) meV/fu in $P3_112$ ($R\bar{3}$) structure. While these results show insignificant numerical differences among the three different structures, a same conclusion can be drawn, that is, with the assistance of Hund's coupling, SOC, electron correlation, and trigonal crystal field, RuCl₃ bulk is in the $S = \frac{1}{2}$ and $L_x = 1$ Mott insulating state.

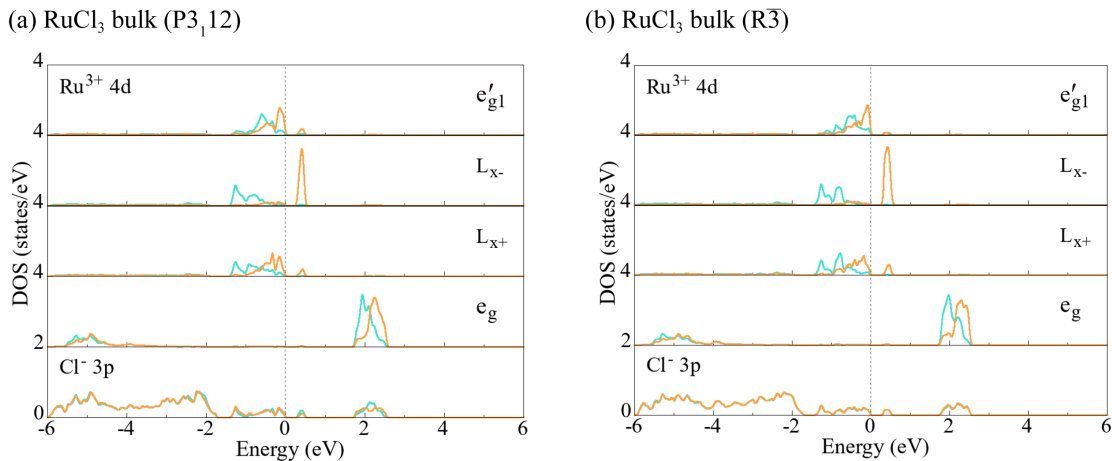


FIG. S1. The DOS results of the $S = \frac{1}{2}$ and $L_x = 1$ zigzag AF state of RuCl₃ bulk in (a) $P3_112$ and (b) $R\bar{3}$ structures by LSDA+SOC+U calculations. The green (orange) curves refer to up (down) spins. The Fermi level is set at zero energy.

II. LSDA+SOC+U and GGA+SOC+U for RuI₃

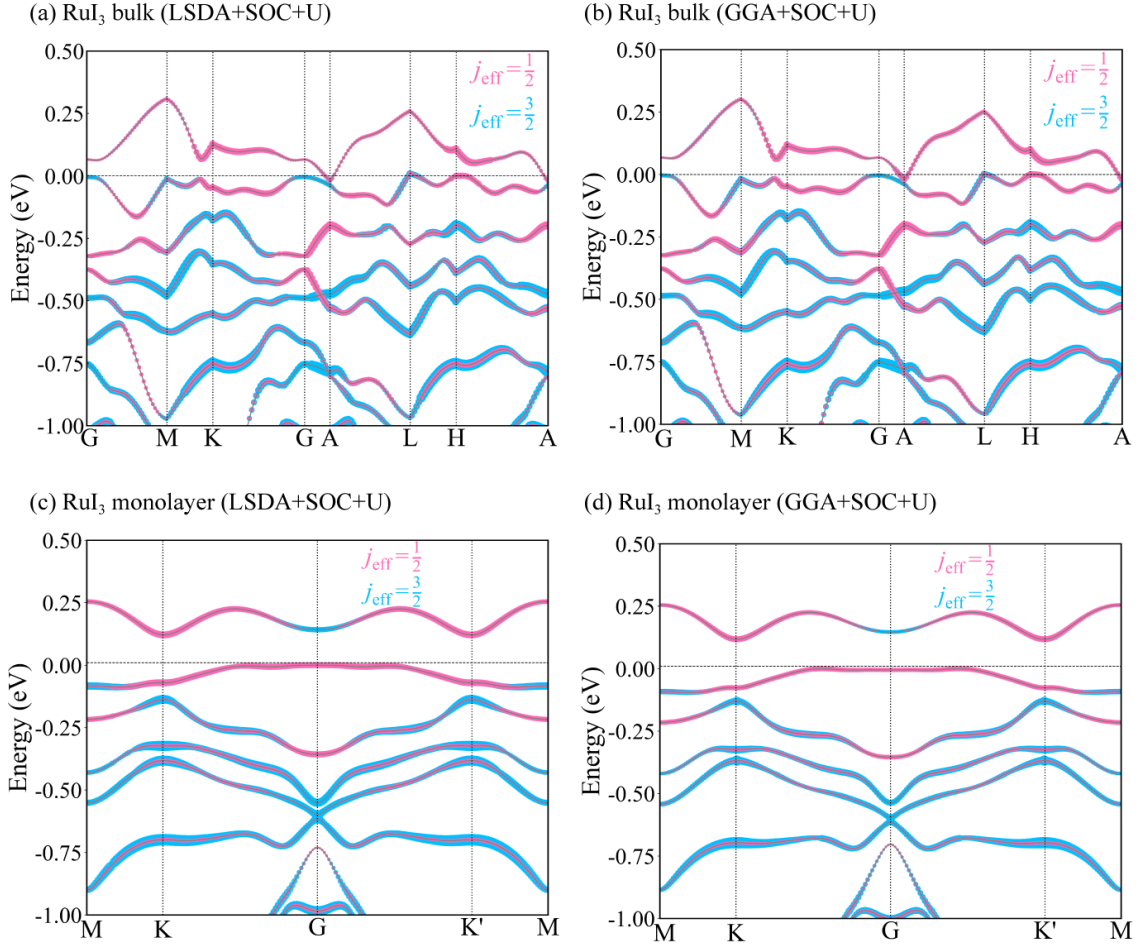


FIG. S2. Band structures for the nonmagnetic state of RuI₃ bulk calculated by (a) LSDA+SOC+U and (b) GGA+SOC+U. Band structures for the nonmagnetic state of RuI₃ monolayer calculated by (c) LSDA+SOC+U and (d) GGA+SOC+U. The pink (blue) curves stand for the $j_{\text{eff}} = \frac{1}{2}$ ($j_{\text{eff}} = \frac{3}{2}$) bands. The Fermi level is set at the zero energy. In both LSDA+SOC+U and GGA+SOC+U calculations, the $j_{\text{eff}} = \frac{1}{2}$ paramagnetic state of RuI₃ bulk and monolayer is obtained and a metal-insulator transition occurs from RuI₃ bulk to monolayer.

III. LSDA+SOC+U and GGA+SOC+U for RuCl_3

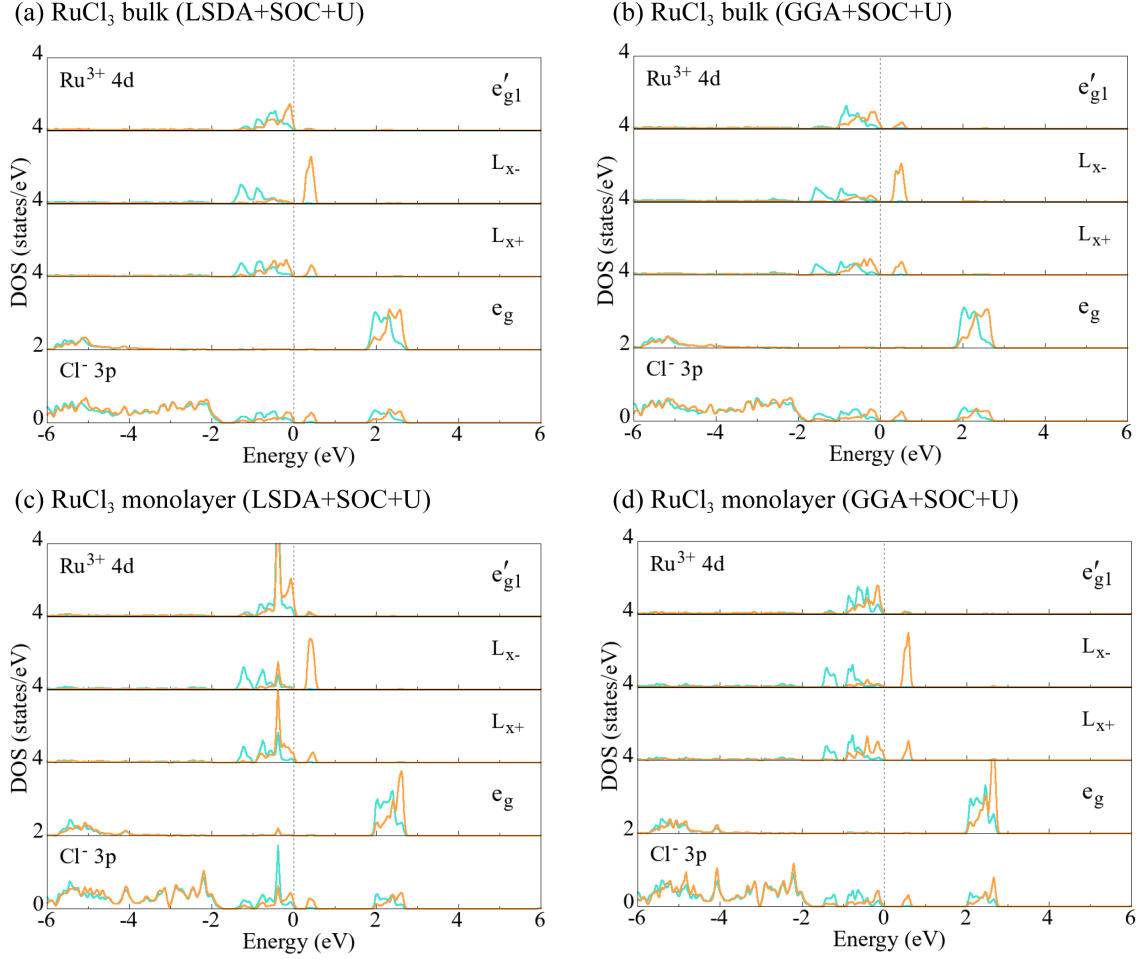


FIG. S3. DOS results for the zigzag AF state of RuCl_3 bulk calculated by (a) LSDA+SOC+U and (b) GGA+SOC+U. DOS results for the zigzag AF state of RuCl_3 monolayer calculated by (c) LSDA+SOC+U and (d) GGA+SOC+U. The green (orange) curves refer to up (down) spins. The Fermi level is set at the zero energy. The local spin/orbital moment of the Ru^{3+} ion in RuCl_3 bulk is calculated to be 0.70/0.47 and 0.75/0.35 μ_B/Ru by LSDA+SOC+U and GGA+SOC+U, respectively. The local spin/orbital moment of the Ru^{3+} ion RuCl_3 monolayer is calculated to be 0.70/0.46 and 0.73/0.43 μ_B/Ru by LSDA+SOC+U and GGA+SOC+U, respectively.

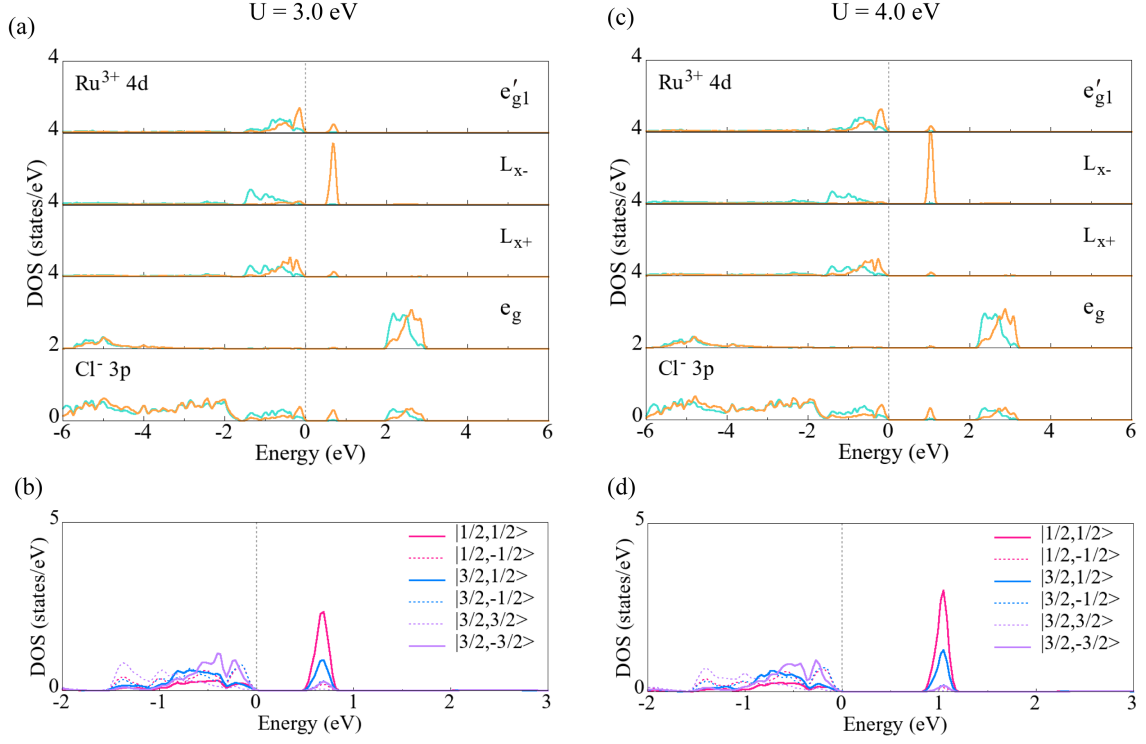
IV. larger U values for RuCl₃ bulk

FIG. S4. DOS results for the zigzag AF state of RuCl₃ bulk, calculated by LSDA+SOC+U with $J_H = 0.5$ eV and U values of (a, b) 3 eV and (c, d) 4 eV. The t_{2g} states in (a) and (c) are projected onto the $|j_{\text{eff}}, m_j^x\rangle$ basis in (b) and (d), respectively. The Fermi level is set at the zero energy. The DOS results closely resemble those shown in Fig. 7, except for the gap size, and all of them support the $S = \frac{1}{2}$ and $L = 1$ Mott insulating state of RuCl₃.